Detonation Wave Propagation in an Ejector-Augmented Pulse Detonation Rocket

Tae-Hyeong Yi*, Donald R. Wilson† and Frank K. Lu†

Aerodynamics Research Center, University of Texas at Arlington, Arlington, TX 76019, USA

The propagation of a detonation wave in an ejector-augmented pulse detonation rocket fueled with a hydrogen-oxygen mixture is studied for a novel concept of a propulsion system. An one- and two-dimensional detonation tube is first investigated to observe the nature of a detonation wave. An interaction between a primary flow from a pulse detonation rocket embedded in a mixing chamber and an incoming secondary flow from an inlet is studied at different incoming Mach numbers. The detonation is initiated by an arc where the ignition conditions are numerically given in an ignition zone with high thermal energy. Two-dimensional, multi-species Euler equations are used with detailed chemistry. The governing equations are discretized using a finite-volume method with a second-order Roe scheme for spatial terms, a second-order, two-step Runge-Kutta method for temporal terms and a time-operator splitting method for source terms. Various features including detonation-shock interaction, detonation diffraction, a base flow and vortex formation are observed.

I. Introduction

Recently, a novel concept of a multi-mode pulse detonation wave based propulsion system for hypersonic flight or single-stage space access has been investigated.[1–3] The main advantage of this conceptual engine is that it operates from takeoff to hypersonic speeds through a single flow path, which should substantially reduce the weight and volume of the vehicle. The engine consists of four modes as illustrated in Fig. 1. Each mode has unique features and operation ranges. For takeoff to moderate supersonic Mach numbers, an ejector-augmented pulse detonation rocket (PDR) embedded in a mixing chamber of the engine is used. This engine mode is similar to a ejector ramjet that uses deflagration combustion. Alike the ejector ramjet, the ejector-augmented PDR provides higher thrust than the regular PDR mounted on a vehicle, by adding momentum to a secondary flow.[4] Moreover, due to the nature of detonation combustion, it also produces higher ejector performance than the ejector ramjet. The purpose of this paper, therefore, is to study the propagation of the detonation wave in the ejector-augmented PDR in order to preliminarily investigate its feasibility as a part of the proposed engine concept.

The investigation of the ejector-augmented PDR mode is divided into two parts. First, a single, isolated one- and two-dimensional detonation tube without a nozzle is simulated to study the propagation of the detonation inside the tube. In the one-dimensional case, the properties of the flow and species for a hydrogen-oxygen mixture is studied. For the case of the two-dimensional tube, the configuration consists of a small initiator tube attached to a larger detonation tube so that several features due to adding the initiator tube may be observed. The detonation wave exhausting from the pulse detonation rocket degenerates into a non-reacting shock wave, which interacts with the secondary flow coming from the inlet in the mixing chamber. Thus, the second investigation on the ejector-augmented PDR is to study the effects of the interaction between the primary and the secondary flows for an incoming Mach number of 0 and 2.5.

The governing equations considered are the Euler equations with source terms due to chemical reactions. Therefore, diffusive effects are neglected and detailed chemistry is involved. To take care of stiffness caused by coupling the fluid dynamics and chemical reactions, time-operator splitting is used in this study. A finite volume method with a cell-centered scheme are employed for space integration, while a second-order,

*Graduate Research Associate, Department of Mechanical and Aerospace Engineering, Student Member AIAA.
†Professor, Department of Mechanical and Aerospace Engineering, Assoc. Fellow AIAA.

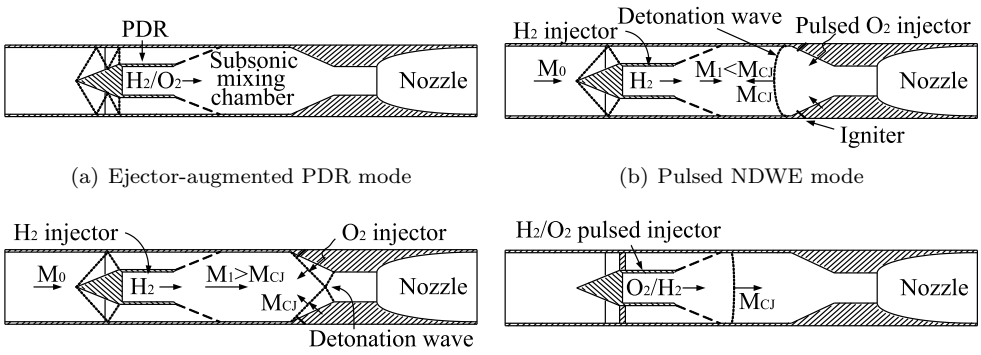

(a) Ejector-augmented PDR mode

(b) Pulsed NDWE mode

(c) Steady ODWE mode

(d) Pure PDR mode

Figure 1. Concept of multi-mode pulse detonation engine

two-step Runge-Kutta method is used for time integration. A system of ordinary differential equations to obtain the chemical source term is solved by a Variable-coefficient Ordinary Differential Equation (VODE) solver.[5] Two chemical reaction mechanisms involved in this study are obtained from GRI-Mech.[6] These mechanisms include twenty-seven elementary reactions with eight species for a hydrogen-oxygen mixture and forty elementary reactions with thirteen species for a hydrogen-air mixture. This paper is based on the dissertation of Yi,[3] where additional details can be found.

II. Mathematical Formulation

A. Governing Equations

The governing equations for a high-temperature, chemically reacting inviscid flow are modeled with thermodynamic processes and chemical reactions as well as the fluid dynamics. Thus, two-dimensional Euler equations are adopted with source terms due to multi-species chemical reactions. These equations are expressed below in a vector form for Cartesian coordinates as[7,8]

$$\frac{\partial \vec{Q}}{\partial t} + \frac{\partial \vec{F}}{\partial x} + \frac{\partial \vec{G}}{\partial y} = \vec{S} \tag{1}$$

where

$$\vec{Q} = \begin{bmatrix} \rho_i \\ \rho u \\ \rho v \\ \rho E \end{bmatrix}, \ \vec{F} = \begin{bmatrix} \rho_i u \\ \rho u^2 + p \\ \rho uv \\ (\rho E + p)u \end{bmatrix}, \ \vec{G} = \begin{bmatrix} \rho_i v \\ \rho uv \\ \rho v^2 + p \\ (\rho E + p)v \end{bmatrix}, \ \vec{S} = \begin{bmatrix} W_i \dot{\omega}_i \\ 0 \\ 0 \\ 0 \end{bmatrix} \tag{2}$$

In the above equations, $i = 1 \cdots N_s$, N_s is the number of species, ρ_i is the density of species i, p is the pressure, u and v are the velocity components, W_i is the molecular weight of species i and $\dot{\omega}_i$ is the mass production rate of species i. The mixture density ρ is determined by the summation of all the species densities in the mixture such as

$$\rho = \sum_{i=1}^{N_s} \rho_i \tag{3}$$

The total energy E is the sum of the internal energy and kinetic energy, that is,

$$E = e + \frac{u^2 + v^2}{2} = h - \frac{p}{\rho} + \frac{u^2 + v^2}{2} \tag{4}$$

A thermally perfect gas is assumed for each species so that the specific heats, enthalpy and internal energy are functions of temperature only. In most practical cases, these thermodynamic properties are approximated by least-square fitting instead of using the kinetic theory. The general forms of the specific

heat at constant pressure in J/(kg · K) and the enthalpy in J/kg are written with least-square coefficients given in the CEA code,[9] respectively, by

$$c_{pi}(T) = \frac{R_u}{W_i}\left(a_1 T^{-2} + a_2 T^{-1} + a_3 + a_4 T + a_5 T^2 + a_6 T^3 + a_7 T^4\right) \tag{5}$$

$$h_i(T) = \frac{R_u T}{W_i}\left(-a_1 T^{-2} + a_2 T^{-1}\ln T + a_3 + a_4\frac{T}{2} + a_5\frac{T^2}{3} + a_6\frac{T^3}{4} + a_7\frac{T^4}{5} + \frac{a_8}{T}\right) \tag{6}$$

The eight coefficients in Eqs. (5) and (6) are presented for each species and these expressions are valid in the temperature range of 200 to 6000 K. The specific heat at constant volume and internal energy of species i are determined from $c_{pi}(T)$ and $h_i(T)$ as

$$c_{vi}(T) = c_{pi}(T) - \frac{R_u}{W_i} \quad \text{and} \quad e_i(T) = h_i(T) - \frac{R_u}{W_i}\,T \tag{7}$$

For the thermodynamic properties of the mixture, the specific heats, enthalpy and internal energy are obtained from their species properties by

$$c_p(T) = \sum_{i=1}^{N_s} Y_i c_{pi}(T) \quad \text{and} \quad c_v(T) = \sum_{i=1}^{N_s} Y_i c_{vi}(T) \tag{8}$$

$$h(T) = \sum_{i=1}^{N_s} Y_i h_i(T) \quad \text{and} \quad e(T) = \sum_{i=1}^{N_s} Y_i e_i(T) \tag{9}$$

where the mass fraction of species i is defined as $Y_i = \rho_i/\rho$. Beside the species thermodynamic properties, the properties for the mixture given in Eqs. (8) and (9) are functions of both the temperature and the mass fraction.

B. Chemical Kinetics

The overall reaction for a stoichiometric hydrogen-air mixture produces water as a result of combustion processes, which is expressed by[10]

$$2\mathrm{H_2} + \mathrm{O_2} + 3.762\mathrm{N_2} \rightarrow 2\mathrm{H_2O} + 3.762\mathrm{N_2} \tag{10}$$

This overall reaction occurs through a series of elementary reactions. The elementary reaction mechanisms for the hydrogen-air and hydrogen-oxygen mixtures are extracted from GRI-Mech 3.0.[6] The mechanism for the hydrogen-air mixture consists of forty elementary reactions with thirteen species (H_2, O_2, N_2, H, HO_2, H_2O, H_2O_2, N, NO, NO_2, N_2O, O and OH), while that for the hydrogen-oxygen mixture consists of twenty-seven elementary reactions with eight species (H_2, O_2, H, HO_2, H_2O, H_2O_2, O and OH). These mechanisms also include parameters for third-body and pressure-dependent reactions. The elementary reaction mechanism can be written in compact form as[10,11]

$$\sum_{i=1}^{N_s} \upsilon'_{ik} X_i \iff \sum_{i=1}^{N_s} \upsilon''_{ik} X_i \quad \text{for } k = 1, 2, \ldots, N_r \tag{11}$$

where the molar concentration of species i is defined as $X_i = \rho_i/W_i$ and the indices i and k denote the number of species and the number of reactions, respectively. In this equation, υ'_{ik} indicates stoichiometric coefficients for the reactants while υ''_{ik} indicates stoichiometric coefficients for the products.

From these elementary reactions, the rate of mass production of species i, which is given in the source terms of Eq. (2), is computed by the summation of all the elementary reactions in the reaction mechanism such as[11]

$$\dot{\omega}_i = \sum_{k=1}^{N_r} \left(\upsilon''_{ik} - \upsilon'_{ik}\right)[\mathrm{M}_i]\left\{k_{f,k}\prod_{i=1}^{N_s}[X_i]^{\upsilon'_{ik}} - k_{r,k}\prod_{i=1}^{N_s}[X_i]^{\upsilon''_{ik}}\right\} \tag{12}$$

where forward rate constant $k_{f,k}$ and reverse rate constant $k_{r,k}$ are obtained from the chemical reaction mechanism and the thermodynamic data table. A third body designated by M_i should appear in Eq. (12) when more energy is released in bonding or required in splitting molecules such as in the case of recombination or dissociation reactions.[10,11] Moreover, the pressure-dependent reactions are also considered in chemical reactions since GRI-Mech[6] provides parameters for such reactions.

III. Numerical Methods

In solving a high-temperature, chemically reacting flow where wide range of time scales is presented, numerical difficulties are encounted due to stiffness. In that case, the chemical reactions have much shorter time scales than those associated with the flow. In order to isolate these stiff source terms presented in Eqs. (1) and (2), time-operator splitting is used in this study. Equation (1) can, therefore, be divided into two steps: (1) a homogeneous partial differential equation for the fluid dynamics and (2) an ordinary differential equation for the chemical reaction:[12,13]

$$\begin{aligned} \text{1st step}: &\quad \frac{\partial \vec{Q}}{\partial t} + \frac{\partial \vec{F}}{\partial x} + \frac{\partial \vec{G}}{\partial y} = 0, \quad \text{IC} : \vec{Q}^n \Rightarrow \vec{Q}^{n+1/2} \\ \text{2nd step}: &\quad \frac{d\vec{Q}}{dt} = \vec{S}, \quad \text{IC} : \vec{Q}^{n+1/2} \Rightarrow \vec{Q}^{n+1} \end{aligned} \tag{13}$$

The governing equations in the first and second step of Eq. (13) are solved successively by following approaches for each step with initial conditions that are obtained from the preceding step. In the first step, a finite volume approach with a cell-centered scheme is employed for space integration. The convective fluxes $\vec{F}$ and $\vec{G}$ given in Eq. (2) at each face of the cell are approximated using the second-order Roe scheme. The original Roe scheme[14] was developed for a calorically perfect gas. This scheme was extended for a multi-species, thermally perfect gas,[12] which is adopted for this study. The Roe scheme also requires to modify the modulus of the eigenvalues since it does not recognize the sonic point so that it produces non-physical expansion waves in the stationary expansion.[15] Thus, the eigenvalues are modified by Harten's entropy correction.[15,16] To obtain second-order accuracy in space, the MUSCL approach[17] is used where the slopes of the linear variations within the cell are limited to prevent nonphysical oscillations around discontinuities such as shock waves. This is done by a minmod limiter function.[18] For spatial terms, the equations are discretized by a second-order, two-step Runge-Kutta method.

The second step in Eq. (13) is a system of ordinary differential equations since it is a function of the species density only at the given temperature, that is,

$$\frac{d\rho_i}{dt} = W_i \dot{\omega}_i \tag{14}$$

This system of ordinary differential equations can be solved using the Variable-coefficient Ordinary Differential Equation (VODE) solver,[5] which takes care of the stiffness problem arising from chemical reactions. Once the species density is updated by VODE in Eq. (14), the temperature must be evaluated at each grid cell.[3,12] It is noted that updating the temperature was also applied to the first step in Eq. (13) as well as to the second step.

IV. One-Dimensional Detonation Tube

A. Physical and Numerical Configuration

The one-dimensional detonation tube has a length of 20 cm. The left end is closed and the right end is open to ambient air at $p = 1$ atm and $T = 300$ K. The tube is initially filled with premixed stoichiometric hydrogen and oxygen gas at initial mole fractions of $C_{\mathrm{H_2}} = 2/3$ and $C_{\mathrm{O_2}} = 1/3$. The initial pressure and temperature in the tube are the same as the ambient air and the mixture is at rest. The mixture is ignited at the left end by an arc, represented numerically as a high pressure and temperature in an ignition zone. The ignition zone is set to $p = 30$ atm and $T = 3000$ K in a 1 mm region, which corresponds to a thermal energy density of 8.152×10^3 J/m^2.

The number of grid points is $N_x = 2000$ so that $\Delta x = 0.1$ mm. At the left end, impervious wall boundary conditions are imposed. At the right end, either a subsonic or a supersonic outflow boundary conditon is applied, depending on the local Mach number at the exit. For subsonic outflow boundary conditions, the ambient pressure of 1 atm is specified at the exit.

B. Results and Discussions

The hydrogen-oxygen mixture exhibits several features over the hydrogen-air mixture where the pressure and temperature in the detonation tube are higher and the detonation wave propagates much faster than

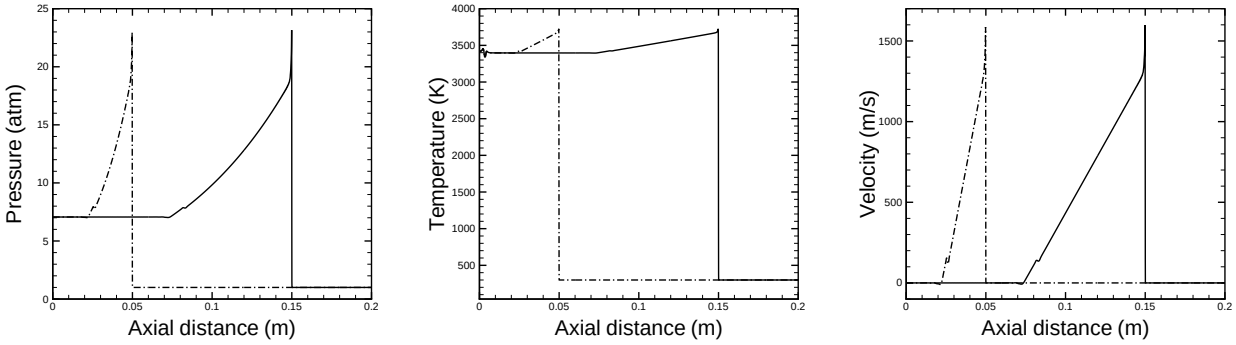

(a) Pressure profiles (b) Temperature profiles (c) Velocity profiles

Figure 2. One-dimensional flow properties in a detonation tube for a stoichiometric H_2/O_2 mixture

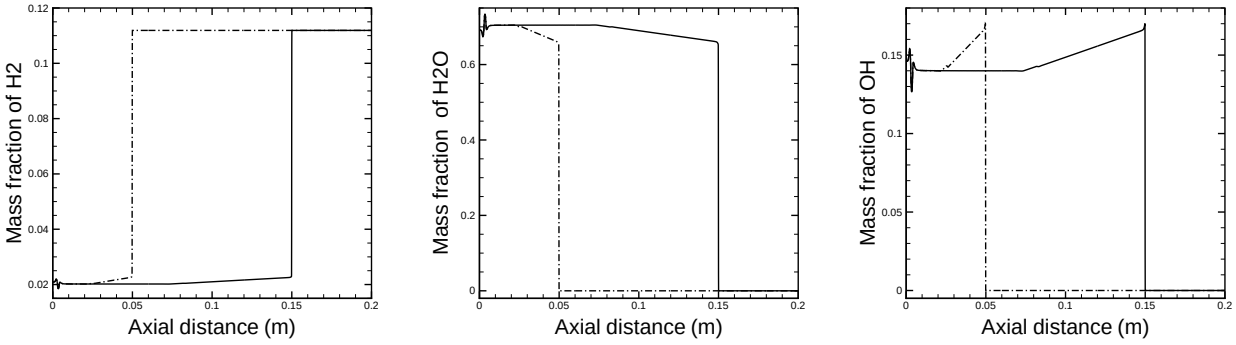

(a) Mass fraction of H_2 (b) Mass fraction of H_2O (c) Mass fraction of OH

Figure 3. One-dimensional species properties in a detonation tube for a stoichiometric H_2/O_2 mixture

for the hydrogen-air mixture. These features are confirmed here. The resulting flow properties and species mass fractions in the one-dimensional detonation tube are presented in Figs. 2 and 3 at $t = 1.7356 \times 10^{-5}$ s and $t = 5.2261 \times 10^{-5}$ s, indicated as dotted and solid lines, respectively. The detonation wave propagation shown in Figs. 2 and 3 is about 2854 m/s, which is closed to the thoeretical CJ detonation velocity of 2843 m/s, obtained from GASEQ.[19] This velocity is much greater than that for a stoichiometric hydrogen-air mixture where the CJ detonation velocity is 1979 m/s.

Figure 2(a) depicts the time evolution of the pressure distribution in the tube, which shows the typical ZND detonation structure such as the leading shock wave, von Neumann pressure spike, CJ pressure and the Taylor rarefaction wave. However, the von Neumann pressure spike is not correctly captured at this grid resolution. It may require a much higher resolution and/or a higher-order numerical scheme[3,20] As the detonation is propagated to the right, the initial pressure on the wall rapidly decays to the pressure of 7 atm and remains constant until the blowdown process occurs in the tube. Figure 2(a) also shows that the pressure distribution behind the leading shock is higher than that for the hydrogen-air mixture.[3] The time evolution of the temperature distribution is given in Fig. 2(b). The computed CJ temperature is approximately 3660 K, which is very close to the theoretical CJ temperature of 3670 K.[19] The temperature behind the shock wave is about 800 K higher than that for the hydrogen-air mixture.[3] Figure 2(c) shows the time evolution of the gas velocity where its theoretical value is 1601 m/s. It is noted that the velocity behind the shock wave decreases to zero in order to match the wall condition.

Figure 3 indicates profiles of the mass fraction of H_2, H_2O and OH for the detonation combustion that converts most of the hydrogen (H_2) and oxygen (O_2) into water vapor (H_2O) and hydroxyl (OH) as combustion products. These four species contribute to roughly 96.2% of the combustion products. The other small contributions for species H, HO_2, H_2O_2 and O to the products were presented by Yi.[3] In Figs. 2 and 3, the detonation wave is initially overdriven but rapidly decreases to below CJ values, and then gradually approaches to the CJ conditions.

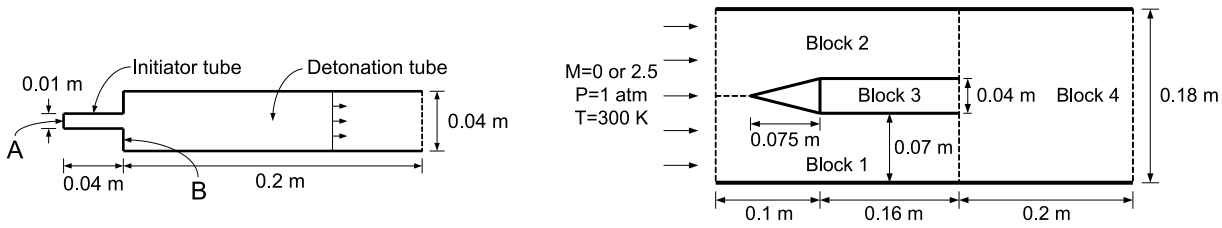

(a) Two-dimensional detonation tube with an initiator (b) Ejector-augmented PDR embedded in a mixing chamber

Figure 4. Physical configurations

V. Two-Dimensional Detonation Tube

A. Physical and Numerical Configuration

A 20 cm long and 4 cm high tube is used for the detonation chamber, while a 4 cm long and 1 cm high tube is used for the initiator as shown in Fig. 4(a). The computational domain is discretized into a total of 134000 grid cells, which corresponds to a cell width of 2.5×10^{-4} m. Two grid blocks are utilized in this case, one for the initiator tube and the other for the detonation tube. Thus, an exchange of flow quantities is required at the interface between the blocks. The wall boundary conditions are applied to the left side of both tubes except at the interface, and subsonic or supersonic outflow conditions are imposed at the right side of the detonation tube, depending on the local Mach number at the exit.

A premixed, quiescent stoichiometric hydrogen-oxygen gas at an ambient pressure of 1 atm and temperature of 300 K is assumed to be filled in both tubes. The mixture is directly ignited with $p = 30$ atm and $T = 3000$ K in a 1 mm long and 10 mm high region at the left side of the initiator. Thus, the planar detonation wave is immediately generated in the initiator.

B. Results and Discussions

The detonation propagation in the initiator and detonation tubes is presented in Fig. 5, which depict the evolution of density gradient. In Fig. 5(a), the detonation wave is propagating in the initiator tube at $t = 6.25474 \times 10^{-6}$ s. At this moment, the pressure in small region behind the reaction zone remains roughly constant and then gradually decreases to match the wall pressure. This is unlike the one-dimensional tube case where the pressure behind the reaction zone immediately decays as shown in Fig. 2(a). Figure 5(b) shows the detonation wave entering the main chamber at $t = 1.59907 \times 10^{-5}$ s, in which a detonation diffraction is observed. This figure indicates a super-critical diffraction[21] where the diameter of the initiator is greater than a critical value so that the detonation is successfully transmitted into the main detonation chamber. As the planar detonation propagates into the main chamber, it becomes cylindrical or spherical. Expansion waves emanate from both edges and propagate into the region behind the leading shock wave.

In an inviscid flow, the flow downstream of a curved shock is rotational, following from Crocco's theorem.[22,23] Thus, a vortex might be generated in an inviscid supersonic flow. This situation occurs in Fig. 5(c) where vortices are generated in the vicinity of the connection section due to the detonation diffraction and the subsequent wave interactions. The vorticity $\vec{\omega}$ is defined in two-dimensional Cartesian coordinates as[22]

$$\vec{\omega} = \nabla \times \vec{w} = \left(\frac{\partial v}{\partial x} - \frac{\partial u}{\partial y} \right) \hat{k} \tag{15}$$

From this equation with the velocity flowfield given in Fig. 5(c), the vorticity magnitude in the vicinity of a connection section is calculated as shown in Fig. 6(a). In Fig. 5(d), the detonation wave becomes planar in the main chamber at approximately $t = 7.31625 \times 10^{-5}$ s and propagates further toward the right open end.

For the two-dimensional detonation tube case, the detonation velocity in the main chamber is computed as about 2833 m/s, which is closed to its one-dimensional and theoretical values. The histories of the pressure measured on the wall of the left sides of the initiator and detonation tube, which is indicated as points A and B in Fig. 4(a), are presented in Figs. 6(b) and (c), respectively. In Fig. 6(b), the pressure on the left wall of the initiator tube initially increases and quickly decays to about 7 atm. It remains constant until

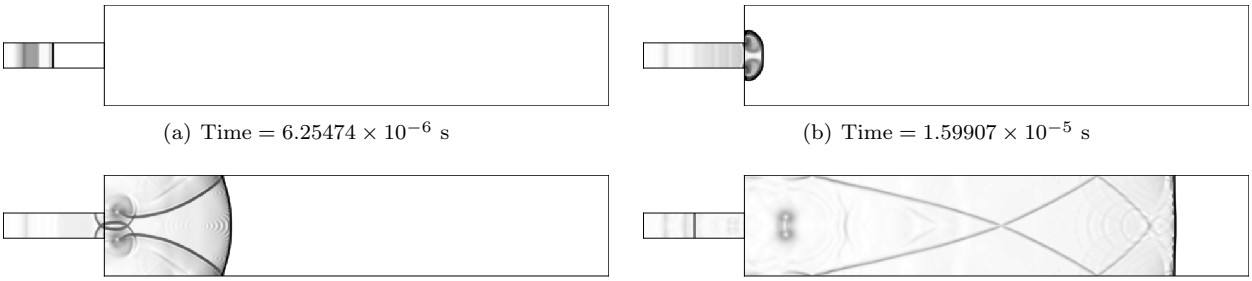

(a) Time = 6.25474×10^{-6} s

(b) Time = 1.59907×10^{-5} s

(c) Time = 3.11758×10^{-5} s

(d) Time = 7.31625×10^{-5} s

Figure 5. Time evolution of the density gradient in the detonation tube

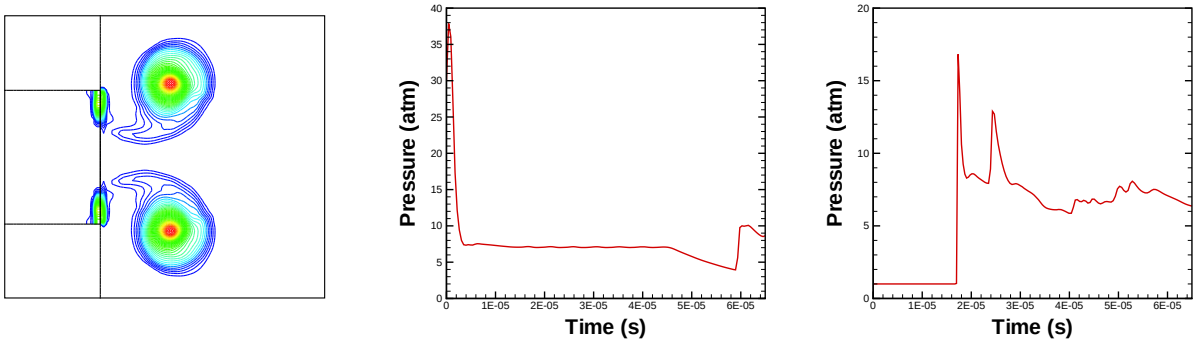

(a) Vorticity magnitude

(b) Pressure at a point A

(c) Pressure at a point B

Figure 6. Vorticity in the vicinity of a connection section and time evolution of the wall pressure

the another set of shock and expansion waves impact the wall. Figure 6(c) shows that the detonation wave reaches the wall of the main detonation chamber at about $t = 1.7 \times 10^{-5}$ s as the first peak. The second peak indicates that shock waves reflected on the upper and lower wall hit the left side of the detonation chamber.

VI. Ejector-Augmented Pulse Detonation Rocket

A. Physical and Numerical Configuration

The investigation of detonation propagation is carried out for an ejector-augmented pulse detonation rocket mode of the multi-mode PDE concept. A slightly shorter detonation tube than that used in the detonation tube cases is utilized with no initiator and it is assumed that a planar detonation wave is generated in the tube for simplicity. The configuration is presented in Fig. 4(b). The incoming air flow is initialized at a pressure of 1 atm, a temperature of 300 K and a Mach number of either 0 or 2.5. The detonation tube is initially filled with a stoichiometric hydrogen-oxygen mixture at the same conditons as the chamber but at rest. Four grid blocks are used in this case. An inert air flow is initially simulated in all the blocks. Once the flow fields are stabilized, the gas in the detonation tube is switched to the hydrogen-oxygen mixture.

B. Results and Discussions

Figures 7 to 10 show the detonation propagation from the tube into the mixing chamber. Pressure and temperature distributions at $M_\infty = 0$ are given in Figs. 7 and 8, respectively. The detonation is initiated at the left side of the tube by an arc so that it is generated and propagated to the right open end. As the detonation propagates into the mixing chamber where only the ambient air exists, the strength of the leading shock weakens and, consequently, the detonation becomes a non-reacting shock wave. Moreover, expansion waves and vortices are generated at the edges of the tube due to detonation diffraction. This situation is presented in Figs. 7(a) and 8(a). In Figs. 7(b) and 8(b), the bow shock wave further propagates upstream and downstream. As a result of the bow shock reflection on the wall, a Mach stem, a slipstream and a triple

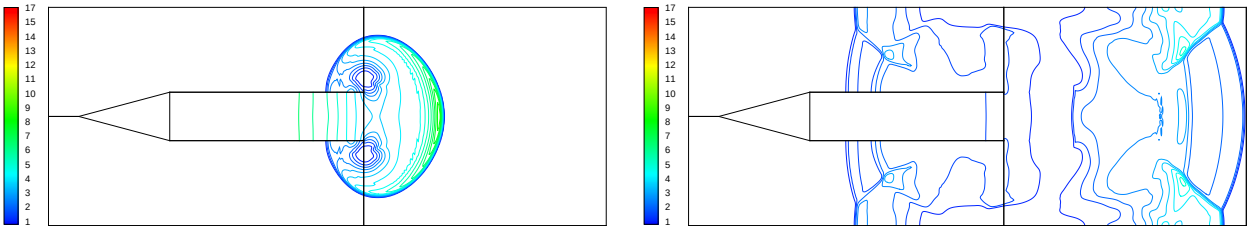

(a) Time = 1.05985×10^{-4} s (b) Time = 2.94958×10^{-4} s

Figure 7. Pressure distribution in the mixing chamber at $M_\infty = 0$

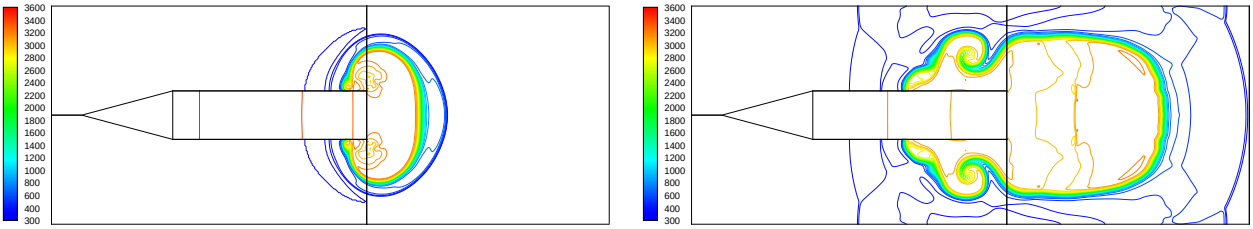

(a) Time = 1.05985×10^{-4} s (b) Time = 2.94958×10^{-4} s

Figure 8. Temperature distribution in the mixing chamber at $M_\infty = 0$

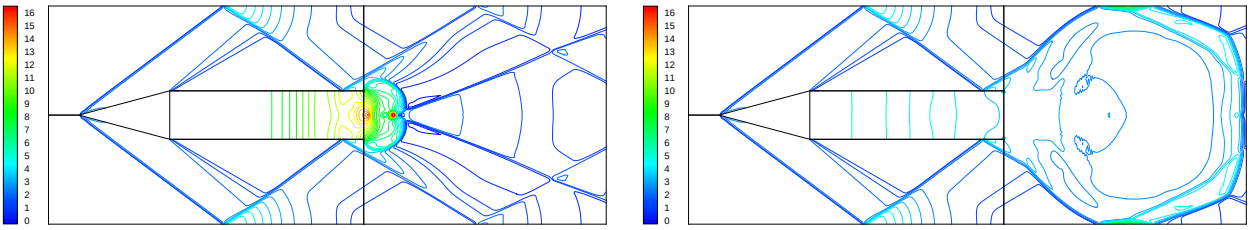

(a) Time = 6.44734×10^{-5} s (b) Time = 1.69463×10^{-4} s

Figure 9. Pressure distribution in the mixing chamber at $M_\infty = 2.5$

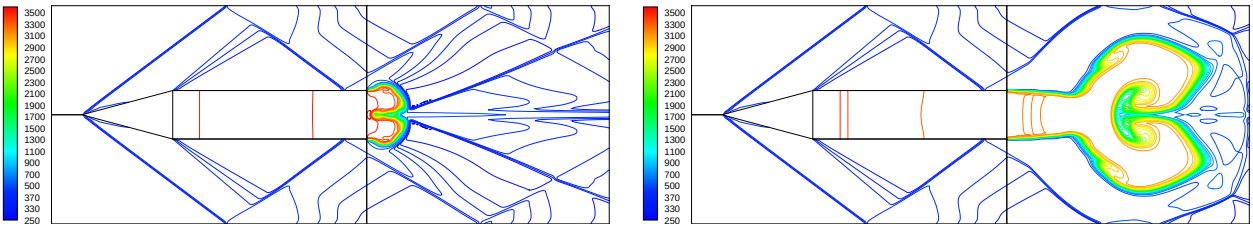

(a) Time = 6.44734×10^{-5} s (b) Time = 1.69463×10^{-4} s

Figure 10. Temperature distribution in the mixing chamber at $M_\infty = 2.5$

point are observed in the figures.

When the velocity of the incoming flow is increased, a more complicated wave structure takes place in the mixing chamber due to the interaction of the primary and secondary flows. Figures 9 and 10 show pressure and temperature distributions in the detonation tube and mixing chamber when the incoming flow is at $M_\infty = 2.5$. A complex shock and expansion system is initially created in the engine. The shock wave emanating from the wedge is reflected at the wall and expansion waves are generated at the tube edges. Typical features of a base flow are observed in Fig. 9(a) and 10(a) such as the low pressure and a reverse flow behind the base, expansion waves due to the large turning angle, the reattachment shock and a locus of the stagnation points.[24] In Fig. 9(b), the shock wave degenerated from the detonation wave propagates into the mixing chamber and interacts with the reattachment shock, resulting in the very high pressure in

the center point of the shock. The high-temperature, primary flow confined by the reattachment shock is separated along the locus of the stagnation points as shown Fig. 10(b).

VII. Conclusions

An ejector-augmented pulse detonation rocket as a part of the multi-mode pulse detonation engine concept was numerically investigated using a computational code. The code modeled an inviscid flow of a thermally perfect and chemically non-equilibrium gas using detailed chemistry. The thermodynamic properties and chemical reaction mechanisms for the hydrogen-oxygen and hydrogen-air mixture are obtained from the CEA and GRI-Mech 3.0 databases, respectively. The ignition of a fuel-oxidizer mixture is accomplished by a simulated arc igniter.

In the one-dimensional tube case, the detonation properties for the hydrogen-oxygen mixture are compared with those for the hydrogen-air mixture. As expected, the hydrogen-oxygen mixture provides a more energetic detonation wave, which propagates much faster. Various physical phenomena are observed in the two-dimensional detonation tube case where the detonation initiator tube is attached to a larger detonation chamber. When the detonation wave in the initiator enters the main tube, it diffracts due to the abrupt area change, resulting in a strong vortex near the transition section. In the case of the ejector-augmented pulse detonation rocket, the detonation wave degenerates into a non-reacting shock wave when it exits the detonation tube. At an incoming Mach number of 2.5 where typical features of a base flow are observed, the shock wave undergoes further interactions with the existing shock-expansion system confined in the mixing chamber.

A more detailed parametric study is required in order to realize the proposed engine concept. No attempt is made to examine the performance of the ejector-augmented pulse detonation rocket in this study. Thus, the effect of a nozzle for the ejector-augmented pulse detonation rocket is recommended for future research. It is also recommended that a two-temperature model be used in the investigation of the high-temperature nozzle flow, since thermal non-equilibrium often occurs in nozzle expansions.

References

[1]Wilson, D. R., Lu, F. K., Kim, H. Y., and Munipalli, R., "Analysis of a Pulsed Normal Detonation Wave Concept," *AIAA paper 2001–1784*, 2001.

[2]Munipalli, R., Shankar, V., Wilson, D. R., Kim, H. Y., Lu, F. K., and Hagseth, P. E., "A Pulsed Detonation Based Multimode Engine Concept," *AIAA 2001-1786*, 2001.

[3]Yi, T. H., *Numerical Study of Chemically Reacting Viscous Flow Relevant to Pulsed Detonation Engines*, Ph.D. thesis, University of Texas at Arlington, Arlington, Texas, 2005.

[4]Heiser, W. H. and Pratt, D. T., *Hypersonic Airbreathing Propulsion*, AIAA Education Series, Washington, DC, 1994.

[5]Brown, P. N., Byrne, G. D., and Hindmarsh, A. C., "VODE: A Variable Coefficient ODE Solver," *SIAM Journal on Scientific and Statistical Computing*, Vol. 10, 1989, pp. 1038–1051, http://www.llnl.gov/CASC/.

[6]Smith, G. P., Golden, D. M., Frenklach, M., Moriarty, N. W., Eiteneer, B., Goldenberg, M., and et al., GRI-Mech 3.0, http://www.me.berkeley.edu/gri_mech.

[7]Anderson, J. D., *Hypersonic and High Temperature Gasdynamics*, McGraw-Hill, New York, 1998.

[8]Kim, H. W., Lu, F. K., Anderson, D. A., and Wilson, D. R., "Numerical Simulation of Detonation Process in a Tube," *Computational Fluid Dynamics Journal*, Vol. 12, No. 2, 2004, pp. 227–2412.

[9]Gordon, S. and McBride, B. J., "Computer Program for Calculation of Complex Chemical Equilibrium Compositions and Application I. Analysis," Tech. Rep. NASA RP–1311, 1976, http://www.lerc.nasa.gov/WWW/CEAWeb.

[10]Turns, S. R., *An Introduction to Combustion: Concepts and Application*, McGraw-Hill, 1996.

[11]Kee, R. J., Coltrin, M., and Glarborg, P., *Chemically Reacting Flow*, Wiley-Interscience, New Jersey, 2003.

[12]Deiterding, R., *Parallel Adaptive Simulation of Multi-Dimensional Detonation Structures*, Ph.D. thesis, Brandenburgische Technische University, Cottbus, Germany, 2003.

[13]Leveque, R. J., *Finite Volume Methods for Hyperbolic Problems*, Cambridge University Press, 2002.

[14]Roe, P. L., "Approximate Riemann Solvers, Parameter Vectors and Difference Schemes," *Journal of Computational Physics*, Vol. 43, No. 2, 1981, pp. 357–372.

[15]Hirsch, C., *Numerical Computation of Internal and External Flows*, Wiley, 1990.

[16]Harten, A. and Hyman, J. M., "Self Adjusting Grid methods for One-dimensional Hyperbolic Conservation Laws," *Journal of Computational Physics*, Vol. 50, 1983, pp. 235–269.

[17]van Leer, B., "Towards the Ultimate Conservative Difference Scheme, V: A Second-Order Sequel to Godunov's Method," *Journal of Computational Physics*, Vol. 32, 1979, pp. 101–136.

[18]Tannehill, J. C., Anderson, D. A., and Pletcher, R. H., *Computational Fluid Mechanics and Heat Transfer*, Taylor and Francis, Washington, D. C., 1997.

[19]Morley, C., "GASEQ: A Chemical Equilibrium Program," http://www.gaseq.co.uk.

[20]Ma, F., *Thrust Chamber Dynamics and Propulsive Performance of Airbreathing Pulse Detonation Engines*, Ph.D. thesis, Pennsylvania State University, University Park, Pennsylvania, 2003.

[21]Schultz, E. and Shepherd, J., "Detonation Diffraction Through a Mixture Gradient," Tech. Rep. FM00-1, California Institute of Technology, 2000.

[22]Emanuel, G., *Analytical Fluid Dynamics*, CRC, 1994.

[23]Yi, T. H. and Emanuel, G., "Unsteady Shock Generated Vorticity," *Shock Waves*, Vol. 10, 2000, pp. 179–184.

[24]Forsythe, J. R., Hoffmann, K. A., Cummings, R. M., and Squires, K. D., "Detached-Eddy Simulation with Compressibility Corrections Applied to a Supersonic Axisymmetric Base Flow," *Journal of Fluids Engineering*, Vol. 124, 2002, pp. 911–923.